

Grazing-Incidence Transmission Small Angle X-Ray Scattering from Thin Films of Block Copolymers

Nikhila Mahadevapuram,¹ Joseph Strzalka,² Gila E. Stein¹

¹Department of Chemical and Biomolecular Engineering, University of Houston, Houston, Texas 77204-4004

²X-Ray Science Division, Argonne National Laboratory, Argonne, Illinois 60439

Correspondence to: G. E. Stein (E-mail: gestein@uh.edu)

Received 20 December 2012; revised 13 January 2013; accepted 15 January 2013; published online 13 February 2013

DOI: 10.1002/polb.23261

ABSTRACT: Thin films of lamellar and cylindrical block copolymers are popular systems for low-cost nanolithography. To be useful as nanoscale templates, the lamellae or cylinders must be oriented perpendicular to the substrate. Domain orientations are usually characterized by microscopy measurements of the film surface, but these techniques cannot detect tilted, bent, or tortuous domains in the film interior. We report a simple method to quantify out-of-plane disorder in thin films of block copolymers based on a variant of grazing-incidence small angle X-ray scattering (GI-SAXS). A typical GI-SAXS experiment illuminates the center of a substrate-supported film at a grazing angle of incidence (near the film/substrate critical angle), and the strong reflected signal is interpreted with the distorted-wave Born approximation. In a new approach, the beam footprint is

moved to the far edge of the sample, allowing the acquisition of a transmission pattern. The grazing-incidence transmission data are interpreted with the simple Born approximation, and out-of-plane defects are quantified through analysis of crystal truncation rods and partial Debye-Scherrer rings. Significantly, this study demonstrates that grazing-incidence transmission small angle X-ray scattering can detect and quantify the buried defect structure in thin films of block copolymers. © 2013 Wiley Periodicals, Inc. *J. Polym. Sci., Part B: Polym. Phys.* **2013**, *51*, 602–610

KEYWORDS: block copolymers; directed self-assembly; grazing incidence small angle x-ray scattering; lithography; SAXS; self-assembly; thin films

INTRODUCTION Thin films of block copolymers are promising systems for low-cost nanoscale lithography.^{1–3} Under thermodynamically favorable conditions, these materials will self-assemble into ordered domains with size and periodicity on the scale of 10–100 nm. The most popular systems for lithography are copolymers that assemble into cylindrical or lamellar phases. To be useful as nanoscale templates, the cylinders or lamellae must be oriented perpendicular to the substrate. This criterion can be difficult to satisfy, because typically one block will prefer to wet the substrate and/or air interface, and this wetting behavior drives a layering of the domains parallel to the interfaces.^{4,5} However, when the block copolymer constituents have similar melt surface tensions, a perpendicular domain orientation can be achieved by tailoring the substrate surface energy with buffer layers.^{6–9} An effective buffer layer is energetically neutral with respect to the copolymer constituents, eliminating the enthalpic drive to form wetting layers at the substrate interface.

Block copolymers based on polystyrene (PS) and poly(methyl methacrylate) (PMMA) constituents are an excellent model system for lithography. PS and PMMA have similar melt surface tensions at elevated temperatures (above 220 °C),^{10–12} so there is little or no tendency to form wetting layers at the air interface.^{13,14} Therefore, by incorporating a substrate buffer layer, perpendicular domain orientations can be sustained

in ultrathin films^{11,15–17} or thick films,¹² depending on the annealing temperature. The in-plane ordering of perpendicular cylinders and lamellae has been studied extensively,^{18,19} and it is known that thermally generated dislocations and disclinations disrupt the lateral correlation lengths.^{20–23} These in-plane defects can be minimized through techniques such as shear alignment,^{24,25} zone refinement,^{26–31} graphoepitaxy,^{32–35} and chemical epitaxy.^{36–42} Out-of-plane defects can distort the size, shape, and positions of desired features,^{43,44} so it is important to develop quantitative methods of characterization. As shown by several literature studies, X-ray and neutron scattering techniques can detect relevant characteristics such as depth-dependent lateral order,^{45–48} out-of-plane domain orientation distributions,^{12,49–51} and depth-dependent domain shape.⁴²

In an earlier work, we examined domain orientations in thin films of PS-PMMA and PMMA-PS-PMMA lamellar copolymers on buffer layers.¹² Using grazing-incidence small angle X-ray scattering (GI-SAXS), we detected a high density of misoriented domains in nearly all of the films we studied. The misorientation angles (relative to the substrate normal) were as large as $(40 \pm 10)^\circ$ in many cases. However, quantitative analysis of GI-SAXS data requires the DWBA, and implementing this theory can be very challenging.^{52,53} In the present work, we demonstrate a simple approach to measure out-of-plane

defects based on grazing-incidence transmission small angle X-ray scattering (GT-SAXS).⁵⁴ This new technique is implemented on a conventional GI-SAXS beam line, but illuminates the edge of the sample with incidence angles that are several times larger than the substrate critical angle. These minor changes to the measurement geometry eliminate the need for complex dynamical scattering models, so quantitative data analysis is quite straightforward. We demonstrate that out-of-plane defects are reliably detected with GT-SAXS, where critical parameters such as the domain orientation and out-of-plane persistence length are calculated from simple analyses of the scattering intensity.

EXPERIMENTAL

Materials

All polymers were purchased from Polymer Source and used as received. Polymer brushes were prepared from a hydroxyl-terminated poly(styrene-co-methyl methacrylate) random copolymer that is 62% styrene with $M_n = 7.0$ kg/mol and polydispersity index (PDI) = 1.3. The lamellar diblock copolymer is poly(styrene-*b*-methyl methacrylate) (PS-PMMA), with $M_n = 100$ kg/mol, PDI = 1.19, and 52% styrene. The equilibrium lamellar periodicity (L_0) is 46 nm, as determined by GI-SAXS. Substrates are single-side polished (100) oriented silicon wafers with minimal bow (per the manufacturer). The wafer thickness is approximately 400 μm . Substrates were cleaned with an ultraviolet light/ozone system to remove organic contamination and grow a thin oxide film (ca. 2 nm). The contact angle of water on clean silicon surfaces is less than 5°.

Substrate Preparation

Random copolymer brush was prepared with a two-stage process that ensures the coating is free of pinholes. The copolymer was dissolved in toluene at a concentration of 1 wt%, and 30-nm thick films were spun-cast on ultraclean silicon substrates. Polymer chains were grafted to the substrate by annealing in a nitrogen-purged glove box for 30 min at 230 °C. Ungrafted polymer was extracted by soaking the samples in toluene for 20–30 min (with gentle agitation), and samples were then dried with nitrogen. The entire process was repeated (for a total annealing time of 1 h). The quality of the brush was evaluated by measuring the contact angle of water, which is typically 77° and consistent with other works.⁶ The brush thickness was measured with a JA Wollam M-2000 spectroscopic ellipsometer. Ellipsometry data were modeled with the Cauchy dispersion relation $n(\lambda) = A + B/\lambda^2$, where A , B , and film thickness are adjustable parameters for regression analysis (all positive values). The calculated Cauchy parameters were $A = (1.50 \pm 0.04)$ and $B = (0.0163 \pm 0.0002)$, and the calculated brush thickness was (3.72 ± 0.3) nm.

Diblock Copolymer Thin Films

Thin films of diblock copolymer with thicknesses $t = (43 \pm 1)$ nm (approximately L_0) and $t = (87 \pm 2)$ nm (approximately $2L_0$) were prepared on the random copolymer brush. Block copolymer was dissolved in toluene at concentrations of 1–2.5

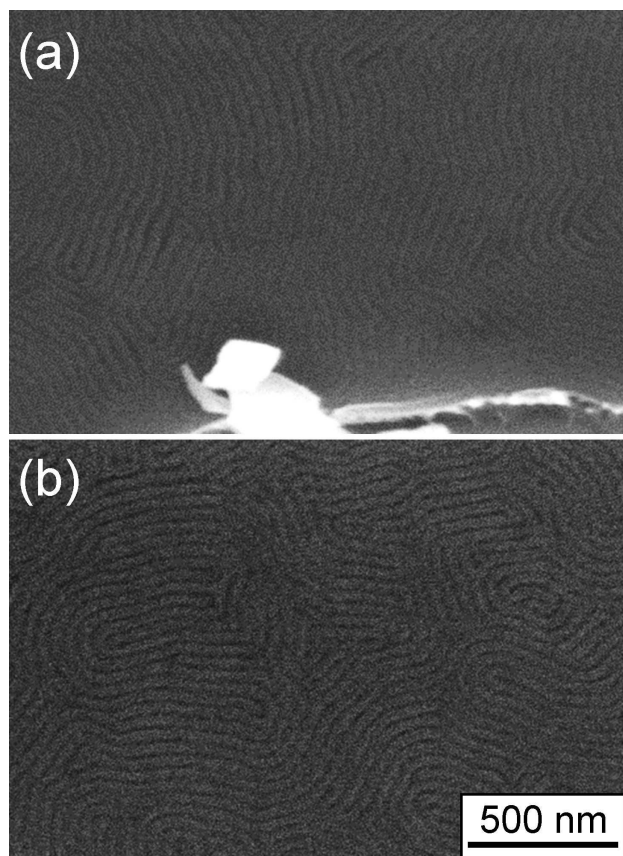


FIGURE 1 SEM images of the block copolymer lamellae at the air interface ($t \approx 2L_0$). (a) Cleaved edge; (b) Center of the silicon wafer.

wt%, and the solution was filtered with a 0.2- μm Teflon mesh. Films were prepared by spin casting at 2000–4000 rpm. Film thicknesses were measured with a JA Wollam M-2000 spectroscopic ellipsometer, and ellipsometry data were modeled with the Cauchy dispersion relation as described in the preceding paragraph. Films were annealed at 240 °C in air for 10 min or under low vacuum (10 mTorr) for 24 h. As discussed in other studies, high temperature/short time annealing in air is more relevant for manufacturing, and the thermal stability of PS-PMMA copolymers is sufficient for these processes.^{12,55} Furthermore, with these processing conditions, commensurability between t and L_0 has little or no impact on out-of-plane order.¹²

Scanning Electron Microscopy

Scanning electron microscopy (SEM) micrographs were collected with a FEI XL-30FEG scanning electron microscope operating at a voltage of 5 keV, current of 0.082 nA, working distance of 4 mm, and 80-kx magnification. An example of these data is included in Figure 1 for a film with thickness of $2L_0$ annealed for 10 min at 240°C; films with thickness L_0 exhibit similar structures at the film surface.

Grazing-Incidence Small Angle X-Ray Scattering

GI-SAXS experiments were conducted at beam line 8-ID-E at the Advanced Photon Source of Argonne National

Laboratory.⁵⁶ Samples were placed in a vacuum chamber and illuminated with unfocused 7.35-keV radiation ($\lambda = 1.68 \text{ \AA}$) at incident angles (α_i) in the range of 0.1–0.7°; the off-specular scattering was recorded with a Pilatus 1MF pixel array detector (pixel size = 172 μm) positioned 2165 mm from the sample. Slit sizes were 50 μm (vertical) and 100 μm (horizontal). Each data set is stored as a 981×1043 32-bit tiff image with 20-bit dynamic range. All data are displayed as intensity maps $I(2\Theta, \alpha_f)$, where 2Θ and α_f denote in-plane and out-of-plane diffraction angles, respectively. The beam footprint was moved toward the far edge of the sample by dropping the z -stage (relative to the incident beam) in increments of 10 μm . Placing the beam at the far edge of the sample enables the recording of transmission data. Acquisition times were approximately 10–60 s per frame for GI-SAXS, and 2–5 min for GT-SAXS. (GT-SAXS measurements require a modestly higher collection time than GI-SAXS due to substrate absorption losses.) The resolution of beam line 8-ID-E is limited by the pixel size of the detector,^{56–58} and this limit is approximately 80 μrad in $2\Theta, \alpha_f$ space. Therefore, all models for the GI-SAXS and GT-SAXS intensity are convolved with a Gaussian resolution function that accounts for this limit.^{57,58}

RESULTS AND DISCUSSION

There are many literature studies where transmission data are observed in GI-SAXS experiments, but these data are serendipitously acquired and rarely analyzed. However, as discussed in a recent manuscript from Lu et al.,⁵⁴ GT-SAXS data are much simpler to interpret than GI-SAXS patterns. These authors demonstrated this approach with nanostructured silicon surfaces, a system with very high scattering contrast. In this article, we report the first demonstration of GT-SAXS from organic materials with weak scattering contrast. We describe the protocols for deliberate acquisition of GT-SAXS data (including sample preparation), summarize the relevant physics, and demonstrate the usefulness of these data for defect analysis in block copolymer thin films.

Grazing-Incidence Small Angle X-Ray Scattering

To illustrate the advantages of grazing-incidence transmission experiments compared with reflection-mode GI-SAXS, we briefly review the salient characteristics of a conventional GI-SAXS experiment. This discussion emphasizes the case of perpendicular block copolymer lamellae, but is generally applicable to any nanostructured film on a reflective surface.

In a typical GI-SAXS experiment, the beam illuminates the center of the sample at a grazing angle of incidence α_i (Fig. 2). (The beam is centered on the sample to ensure that all the incident radiation is intercepted by the sample, which maximizes the signal-to-noise.) To sample the full film thickness, the incident angle must be larger than the polymer's critical angle and smaller than the substrate's critical angle, that is, $\alpha_{c,p} < \alpha_i < \alpha_{c,s}$. Under this condition, the incident beam is transmitted at the air-polymer interface, penetrates the full film thickness, and is largely reflected from the substrate. Shallow incidence angles

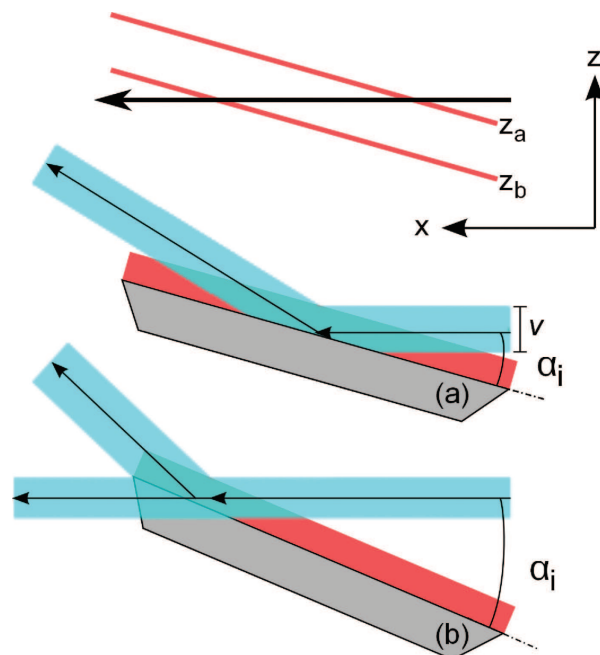


FIGURE 2 (a) GI-SAXS and (b) GT-SAXS scattering geometry. For GT-SAXS, the beam footprint is moved to the far edge of the sample by dropping the sample position along the z -axis.

will generate a long-beam footprint (10's of mm), so there are many transmitted and reflected beams that propagate and interfere within the film. The interference produces standing waves inside the film that enhance the GI-SAXS intensity when α_f is similar to the film and substrate critical angles. Furthermore, the internal microstructure (lamellar domains) will scatter the transmitted and reflected beams. These scattering events are incoherent, as typical block copolymer films are characterized by poor lateral order. The different types of scattering events are illustrated in Figure 3 and discussed in numerous references.^{46,51,54,59,60}

We simulate the GI-SAXS intensity for lamellar copolymer films using the DWBA, following procedures described elsewhere^{46,48,61}:

$$I(q_x, q_y, q_z) \propto |T^f T^i P(q_{\text{par}}, q_{z1}) S(q_{\text{par}}, q_{z1}) + T^f R^i P(q_{\text{par}}, q_{z2}) S(q_{\text{par}}, q_{z2}) + T^i R^f P(q_{\text{par}}, q_{z3}) S(q_{\text{par}}, q_{z3}) + R^f R^i P(q_{\text{par}}, q_{z4}) S(q_{\text{par}}, q_{z4})|^2 \quad (1)$$

The coefficients T^f , T^i , R^f , and R^i are the amplitudes of the transmitted and reflected waves, where the superscripts f and i denote outgoing and incoming waves, respectively. These coefficients are calculated from the Parratt recursions.⁶² The in-plane scattering vector is $q_{\text{par}} = \{q_x^2 + q_y^2\}^{0.5} \simeq q_y$. The out-of-plane scattering vectors q_{z1} , q_{z2} , q_{z3} , q_{z4} are a function of

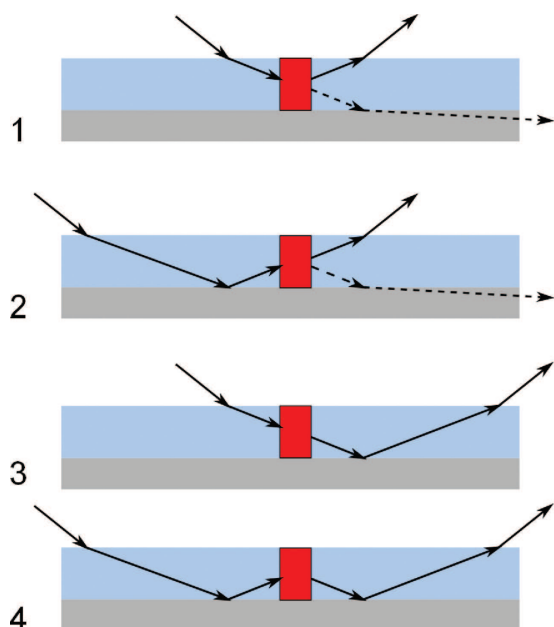


FIGURE 3 Four possible scattering events in a typical GI-SAXS experiment. The solid lines denote the incoming and outgoing waves for GI-SAXS, whereas the dashed lines represent the GT-SAXS experiment.

the scattered (k_z^f) and incident (k_z^i) wave vectors, corrected for refraction at the polymer–air interface:

$$q_{z1} = k_z^f - k_z^i \quad (2)$$

$$q_{z2} = k_z^f + k_z^i \quad (3)$$

$$q_{z3} = -k_z^f - k_z^i \quad (4)$$

$$q_{z4} = -k_z^f + k_z^i \quad (5)$$

$$k_z^f = 2\pi \left\{ \sin^2 \alpha_f - \sin^2 \alpha_{c,p} \right\}^{0.5} / \lambda \quad (6)$$

$$k_z^i = -2\pi \left\{ \sin^2 \alpha_i - \sin^2 \alpha_{c,p} \right\}^{0.5} / \lambda \quad (7)$$

The function $P(\mathbf{q})$ is the lamellar form factor,

$$P(\mathbf{q}) = 4 \frac{\sin(q_y w)}{q_y} \frac{\sin(q_z h/2)}{q_z} \exp \left\{ -\frac{i q_z h}{2} \right\}, \quad (8)$$

where w and h are the domain half-width and height, respectively, and the scattering vector is $\mathbf{q} = \{q_x, q_y, q_z\}$. The function $S(\mathbf{q})$ is the structure factor for a one-dimensional lamellar system, that is, $S(\mathbf{q}) = \sum_n \delta(q_y - 2\pi n/L_0)$.

If the lamellar orientation is perfectly perpendicular to the substrate (Fig. 4), then the GI-SAXS intensity is simulated with the model described by eqs 1 and 8.⁶³ Within this framework, the diffuse scattering is concentrated into crystal truncation rods (CTRs) with strong form factor oscillations along the α_f axis, where the oscillation period scales with the inverse of the lamellar height h . Furthermore, the model predicts strong enhancement of the GI-SAXS intensity at exit angles near the substrate critical angle. These features are called Yoneda peaks, and they are associated with standing waves inside the film.⁶⁴

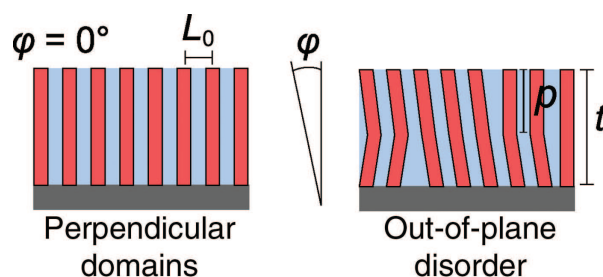


FIGURE 4 Illustration of lamellar copolymer films with perpendicular domain orientations and out-of-plane disorder. The parameter p denotes the (average) persistence length of the perpendicular lamellae, whereas ϕ denotes the full range of tilt angles (inclusive).

Figure 5(a,b,d,e) reports GI-SAXS measurements for films with thicknesses $t \simeq L_0$ and $t \simeq 2L_0$ that were annealed for 10 min. We observe the predicted CTRs and Yoneda peaks. However, we also observe shoulders on each CTR at low angles, which could be partial Debye–Scherrer rings.^{12,60} Debye–Scherrer rings are associated with out-of-plane orientation disorder such as tilted or bent domains (Fig. 4). The partial Debye–Scherrer rings are simulated by including an orientation distribution function in the DWBA model. The total intensity is modeled with the local monodisperse approximation, where we sum the (incoherent) scattering from monodisperse regions, and weight these contributions by the domain orientation distribution. Both the form factor and structure factor are corrected for the tilt angle ϕ , which is defined relative to the substrate normal as illustrated in Figure 4. The form factor for a tilted lamellar domain is

$$P(\mathbf{q}) = \int_{-h/2}^{+h/2} \int_{-w-z \tan \phi}^{+w-z \tan \phi} \exp \{ -i(q_y y + q_z z) \} dy dz. \quad (9)$$

Note that the integral in eq 9 has a (long) analytic solution. The structure factor is also corrected for the tilt angle ϕ , that is, $S(\mathbf{q}) = \sum_n \delta(|\mathbf{q} - R_\phi \cdot \mathbf{q}_B|)$, where R_ϕ is a rotation matrix and $\mathbf{q}_B = \{0, 2\pi n/L_0, 0\}$.

Figure 5(c,f) reports the simulated GI-SAXS data for each film thickness. The simulations assume that 75% of the film volume contains perpendicular lamellar domains, and the remaining 25% of the film is characterized by out-of-plane orientation disorder. For the perpendicular domains, we assume the lamellar height is $h = t$, meaning the lamellae persist through the entire film thickness. For the domains with orientation disorder, we apply a Gaussian orientation distribution with a standard deviation of $\sigma_\phi = 10^\circ$. The simulations qualitatively agree with the experiments.

There are two limitation with the GI-SAXS data analysis. First, as film thickness is increased, the form factor oscillations along the first-order CTR become significantly compressed and are difficult to resolve. Therefore, it is difficult to ascertain if the perpendicular lamellae propagate throughout the film thickness, or if they are somewhat truncated in the film interior. These compressed features are clearly observed in Figure

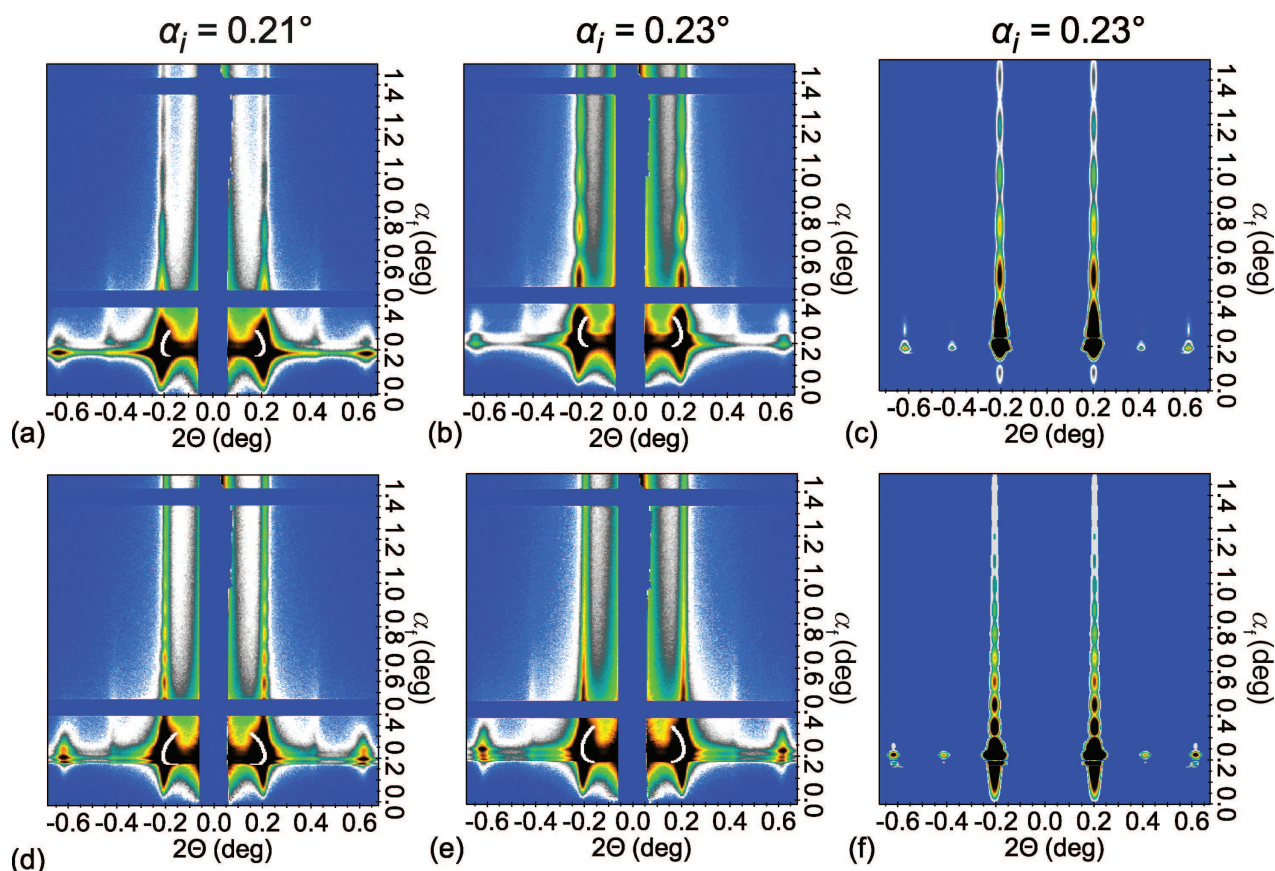


FIGURE 5 (a,b) Measured GI-SAXS data for a film of thickness $t \simeq L_0$, 10-min anneal, incident angles of $\alpha_i = 0.21^\circ$ and $\alpha_i = 0.23^\circ$, 10-min anneal. (c) Simulated GI-SAXS data for a film of thickness $t \simeq L_0$. (d,e) Measured GI-SAXS data for a film of thickness $t \simeq 2L_0$, incident angles of $\alpha_i = 0.21^\circ$ and $\alpha_i = 0.23^\circ$. The white contours mark the trajectory of partial Debye–Scherrer rings, with $\sigma_\phi = 10^\circ$. (f) Simulated GI-SAXS data for a film of thickness $t \simeq 2L_0$. The white contours in (a,b,d,e) mark the trajectory of predicted partial Debye–Scherrer rings, with $\sigma_\phi = 10^\circ$. Simulations in (c,f) assume a mixture of perpendicular domains (75 vol%) and out-of-plane disorder (25 vol%), where the perpendicular persistence length is fixed at $h = t$, and the out-of-plane disorder assumes $\sigma_\phi = 10^\circ$.

5(d–f) (samples with $t \simeq 2L_0$). Second, refraction of incoming and outgoing beams will compress the Debye–Scherrer ring along the α_f -axis, making it difficult to distinguish this feature from the much stronger Yoneda peaks. For example, referring to Figure 5, it is unclear if these data contain a partial ring or merely a broad line shape that is enhanced by the standing waves. These complications are mitigated with grazing-incidence transmission measurements, which is discussed in the next section of this article.

Grazing–Incidence Transmission Small Angle X-Ray Scattering

To acquire transmission data, the beam must exit the far edge of the film as illustrated in Fig. 2. There are several ways to move the footprint to the far edge of the sample. For example, one could expand the vertical slits (v in Fig. 2) to increase the length of the footprint, move the sample upstream along the x -axis, or move the sample down the z -axis. For the beamline in question, the z -axis approach illustrated in Figure 2 was the simplest and most reliable.⁶⁵ The protocol for positioning the footprint is straightforward: the sample is dropped along the

z -axis in increments of 10 μm , and the scattering is recorded for 1 s. The “optimal” z -position is selected by maximizing the intensity of the transmission pattern. The alignment process is complete in about 1 min. The attenuation length for 7.35-keV radiation in silicon is approximately 50 μm , so the beam is penetrating the silicon wafer as illustrated in Figure 2, and the path length for recorded data is on the order of 10 μm (depending on the angle of incidence).

There are two important considerations when preparing samples for GT-SAXS measurements. First, the sample “edge” should be smoothly cleaved silicon, because parasitic scattering from a jagged structure will obscure the low-angle data. (A beveled edge will block the GT-SAXS signal entirely.) Second, the cleave must be made after spin-coating the film to remove the edge bead and other spin-cast defects, because thickness variations will affect the domain orientations. Using SEM measurements (Fig. 1), we find that cleaving the sample does not damage the lamellar morphology—the film is intact at the edge, and the lamellar structure is preserved. Figure 6(a,b) compares GT-SAXS measurements before and after cleaving the wafer to remove regions with thickness variation,

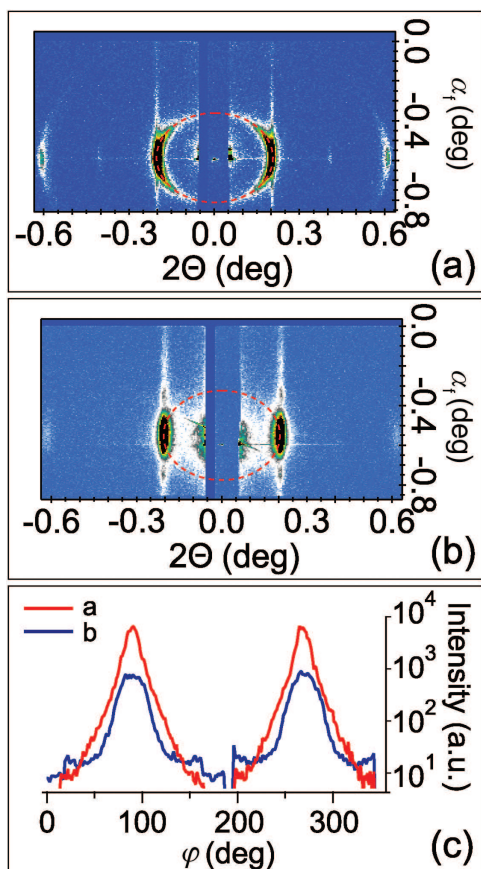


FIGURE 6 Measured GT-SAXS data for (a) sample with thickness variation within the footprint; (b) sample with uniform film thickness of $t \simeq 2L_0$. The azimuthal intensity profile from parts (a) and (b) are reported in (c).

and Figure 6(c) reports the azimuthal integration of the scattering intensity. When we measure samples with thickness variation due to spin casting defects, the GT-SAXS signal is almost always characterized by a partial or complete Debye-Scherrer ring. This means the thick block copolymer rim at the sample edge contains a large population of misoriented lamellae. When we measure the cleaved samples that have a uniform film thickness at the edge, the GT-SAXS signal does not contain the broad Debye-Scherrer rings. Instead, we observe the form factor for perpendicular lamellae, where the broad in-plane peak shape is associated with the small grain size in the lamellar film (see Fig. 1).

Our aim is to quantify the out-of-plane structure in block copolymer films through analysis of GT-SAXS data. Referring back to eq 1 and Figure 3, we note that the scattering from Conditions 3 and 4 are well-separated from the GT-SAXS signal for sufficiently large α_i .⁵⁴ Furthermore, when α_i is much larger than $\alpha_{c,s}$, then the reflection coefficient R^i is approximately 0 (Condition 2 vanishes) and $T^f T^i \approx \text{constant}$ (unity). In this limit, the scattering is described by the simple Born approximation,

$$I(\mathbf{q}) \propto |P(\mathbf{q})S(\mathbf{q})|^2. \quad (10)$$

Refraction corrections are included for the incident beam at the air-polymer interface, and the transmitted beam at the polymer-substrate interface. The beam exits the far edge of the silicon substrate at a large angle (near normal incidence), so refraction corrections are neglected. The x , y , and z components of the scattering vector for this geometry are^{54,60},

$$q_x = k_0 \{ \cos \alpha_f \cos 2\Theta - \cos \alpha_i \} \quad (11)$$

$$q_y = k_0 \{ \cos \alpha_f \sin 2\Theta \} \quad (12)$$

$$q_z = k_z^f - k_z^i \quad (13)$$

$$k_z^f = -2\pi \{ \sin^2 \alpha_f + \sin^2 \alpha_{c,s} - \sin^2 \alpha_{c,p} \}^{0.5} / \lambda \quad (14)$$

$$k_z^i = -2\pi \{ \sin^2 \alpha_i - \sin^2 \alpha_{c,p} \}^{0.5} / \lambda \quad (15)$$

We used an incident angle of at least 0.6° for our GT-SAXS measurements, which is approximately three times larger than the critical angle of silicon (0.245° at 7.35 keV). With $\alpha_i = 0.6^\circ$, the reflection coefficient R^i is on the order of 10^{-1} and $T^f T^i \approx \text{constant}$.⁶⁶ Therefore, we simulate the GT-SAXS patterns using the Born approximation. If the lamellar orientation is perfectly perpendicular to the substrate (Fig. 4), then we observe CTRs-like those detected in a GI-SAXS measurement. These patterns are simulated with the form factor defined by eq 8.⁶³ If the perpendicular lamellae are truncated in the film interior, then we include height polydispersity using the local monodisperse approximation, where the incoherent scattering from different persistence lengths is weighted by a Gaussian distribution. If the film contains tilted domains, then we observe the partial Debye-Scherrer rings in addition to the CTRs. The partial rings are simulated with the “tilted” form factor described by eq 9 using the local monodisperse approximation.

Figure 7 reports a comparison between measured and simulated GT-SAXS patterns for films with thicknesses $t \simeq L_0$ and $t \simeq 2L_0$. Additionally, we report the best-fit of the first-order CTR intensity to the GT-SAXS model, and the azimuthal intensity profile along the predicted Debye-Scherrer contour. For both film thicknesses, we find that the average lamellar persistence length is less than the film thickness, that is, $p < t$. First, with regards to the $t \simeq L_0$ system, we find the average lamellar persistence length is $0.5 L_0$. This implies that 50% of the film contains out-of-plane orientation defects, or the film was locally thinner than the average value due to a spin-casting defect. The in-plane line shape of the CTR is quite broad, so it is difficult to detect any misoriented domains through an azimuthal integration—which means that $\sigma_\phi < 20^\circ$ for this sample. The GI-SAXS measurements for this sample were consistent with a lamellar persistence length near L_0 , so we speculate that the GT-SAXS data were acquired from a defective patch of the film. The small sampled area in a GT-SAXS experiment relative to a GI-SAXS experiment has advantages and disadvantages; one can profile heterogeneities in the film structure, which is advantageous for applications in nanopatterning, but the local measurement might not represent the average film structure. Second, for the $t \simeq 2L_0$ system, we find significant polydispersity in the persistence length of perpendicular lamellae, and we detect asymmetry in the peak line

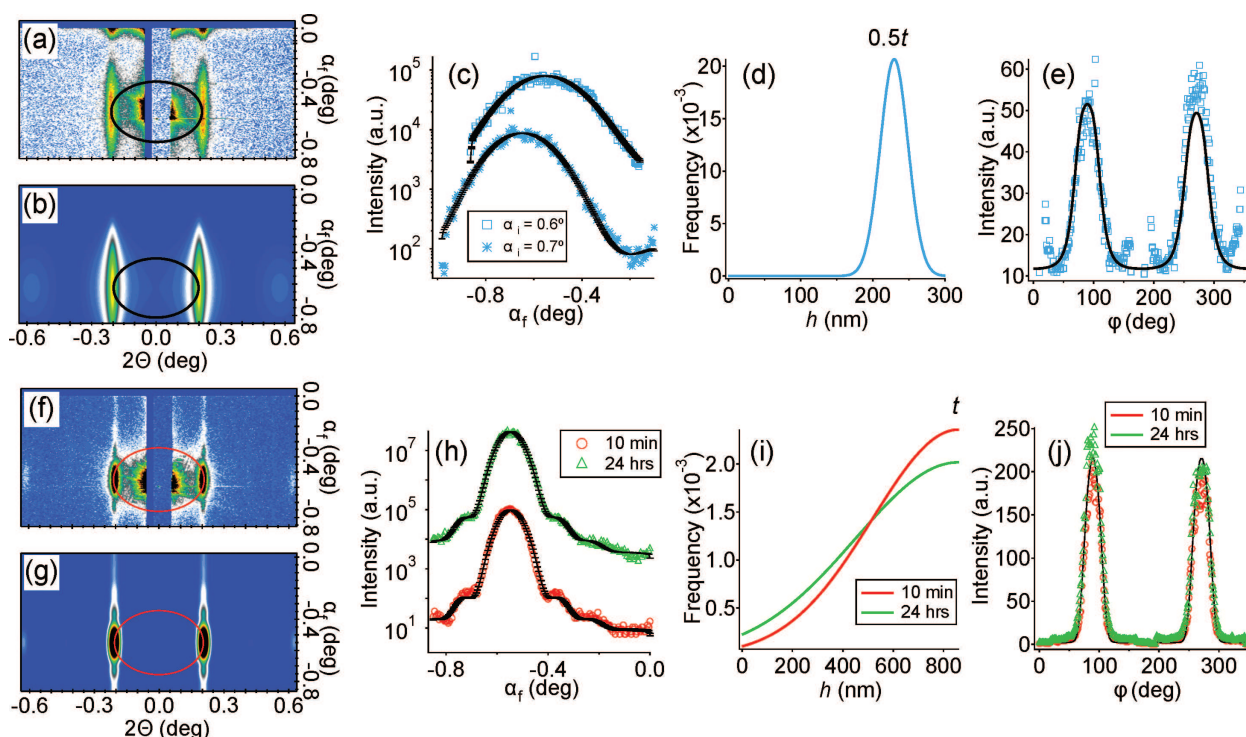


FIGURE 7 (a,b) Measured and simulated GT-SAXS data for $t \approx L_0$, 10-min anneal. (c) CTR and best-fit to GT-SAXS model for $t \approx L_0$, 10-min anneal. (d) Best-fit lamellar height distribution for $t \approx L_0$, 10-min anneal. (e) Simulated and measured azimuthal profile for $t \approx L_0$, 10-min anneal. (f,g) Measured and simulated GT-SAXS data for $t \approx 2L_0$, 10-min anneal. (h) CTR and best-fit to GT-SAXS model for $t \approx 2L_0$, 10-min and 24-h anneal. (i) Best-fit lamellar height distribution for $t \approx 2L_0$, 10-min and 24-h anneal. (j) Simulated and measured azimuthal profile for $t \approx 2L_0$, 10-min and 24-h anneal. Incident angles are $\alpha_i = 0.6^\circ$ unless otherwise noted. Error bars encompass the 95% confidence interval.

shape that is consistent with out-of-plane orientation defects. We report data for 10 min and 24-h annealing, and these cases are nearly identical. From analysis of the CTR, we find the dominant persistence length is similar to the film thickness, which is consistent with the GI-SAXS analysis of the same samples. From analysis of the azimuthal profile, we estimate that 30% of the film volume is characterized by out-of-plane disorder, where $\sigma_\phi \approx (15 \pm 5)^\circ$. These preliminary data suggest that prolonged annealing will not remove the out-of-plane defects, which is consistent with a prior work from our group.¹²

Considering the simplicity of both the experiment and data analysis, we expect that GT-SAXS will be very valuable for quantifying out-of-plane defects in thin films of block copolymers. The technique is not restricted to perpendicular lamellae or cylinders; tilted planes of parallel cylinders, layered spheres, or perforated lamellae can also be measured with this approach. If a higher beam energy were used, then the silicon substrate would have greater transparency and the sampled film volume would increase, thereby improving the signal-to-noise. In such a case, the higher-order CTRs could be detected, so one could measure the depth-dependent shape of the domains.⁴²

We have not discussed the physical origins of out-of-plane defects in block copolymer films, but understanding this phenomena is the subject of ongoing work in our group.¹² At the

present time, we believe that interactions between the block copolymer and underlying surface might pin these defects.⁶⁷ Within this view, the perpendicular domains extend from the air interface into the film interior; and then “bend” near the substrate interface. Further studies are needed to validate this hypothesis. Ultimately, our goal is to determine the optimal design of buffer layers for block copolymer lithography.

CONCLUSIONS

Block copolymer lithography is among the leading candidates for next-generation lithography in the semiconductor industry. Out-of-plane disorder in a block copolymer template will induce significant errors in feature size and placement, but detecting and minimizing these defects is very challenging. We demonstrate that GT-SAXS can detect out-of-plane defects in block copolymer films. This approach is simple, fast, and provides a quantitative measure of persistence lengths and orientation distributions in lamellar copolymers. These data can provide feedback to optimize a self-assembly process. Furthermore, these data also demonstrate that GT-SAXS can measure organic materials with weak x-ray contrast, and GT-SAXS can be implemented with a relatively low photon energy (7.35 keV).

As a secondary point, we note that many literature studies infer a perpendicular domain orientation based on microscopy

measurements of the film surface. Clearly, techniques such as atomic force microscopy and SEM are more readily available to most researchers than a GI-SAXS line. However, numerous works have demonstrated that domain ordering at the free surface can be very different from the behavior at a substrate interface.^{19,45,47,49,50,68,69} Furthermore, top-down microscopy cannot distinguish between perpendicular, tilted, bent, truncated, or tortuous domain orientations. Therefore, we believe that microscopy data should be interpreted with caution, and other metrologies could better guide the development and optimization of block copolymer lithography.

ACKNOWLEDGMENTS

N.M. and G.E.S. acknowledge financial support by the Norman Hackerman Advanced Research Program under Grant No. 003652-0017-2011. Use of the Advanced Photon Source was supported by the U.S. Department of Energy, Office of Science, Office of Basic Energy Sciences, under Contract No. DE-AC02-06CH11357. The authors thank Ben Ocko for sharing an advance copy of his manuscript.

REFERENCES AND NOTES

- R. A. Segalman, *Mater. Sci. Eng. R Rep.* **2005**, *48*, 191–226.
- C. T. Black, R. Ruiz, G. Breyta, J. Y. Cheng, M. E. Colburn, K. W. Guarini, H.-C. Kim, Y. Zhang, *IBM J. Res. Dev.* **2007**, *51*, 605–633.
- J. Bang, U. Jeong, D. Ryu, T. Russell, C. Hawker, *Adv. Mater.* **2009**, *21*, 4769–4792.
- M. J. Fasolka, A. M. Mayes, *Ann. Rev. Mater. Res.* **2001**, *31*, 323–355.
- M. W. Matsen, *J. Chem. Phys.* **1997**, *106*, 7781–7791.
- P. Mansky, Y. Liu, E. Huang, T. P. Russell, C. J. Hawker, *Science* **1997**, *275*, 1458–1460.
- P. Mansky, T. P. Russell, C. J. Hawker, M. Pitsikalis, J. Mays, *Macromolecules* **1997**, *30*, 6810–6813.
- D. Y. Ryu, K. Shin, E. Drockenmuller, C. J. Hawker, T. P. Russell, *Science* **2005**, *308*, 236–239.
- S. Ji, C.-C. Liu, J. G. Son, K. Gotrik, G. S. W. Craig, P. Gopalan, F. J. Himpsel, K. Char, P. F. Nealey, *Macromolecules* **2008**, *41*, 9098–9103.
- P. Mansky, T. P. Russell, C. J. Hawker, J. Mays, D. C. Cook, S. K. Satija, *Phys. Rev. Lett.* **1997**, *79*, 237–240.
- E. Han, K. Stuen, M. Leolukman, C. C. Liu, P. Nealey, P. Gopalan, *Macromolecules* **2009**, *42*, 4896–4901.
- T. Vu, N. Mahadevapuram, G. M. Perera, G. E. Stein, *Macromolecules* **2011**, *44*, 6121–6127.
- G. Coulon, T. P. Russell, V. R. Deline, P. F. Green, *Macromolecules* **1989**, *22*, 2581–2589.
- G. Coulon, B. Collin, D. Ausserre, D. Chatenay, T. P. Russell, *J. Phys.* **1990**, *51*, 2801–2811.
- S. Ham, C. Shin, E. Kim, D. Y. Ryu, U. Jeong, T. P. Russell, C. J. Hawker, *Macromolecules* **2008**, *41*, 6431–6437.
- E. Han, K. O. Stuen, Y. H. La, P. F. Nealey, P. Gopalan, *Macromolecules* **2008**, *41*, 9090–9097.
- H. S. Suh, H. Kang, C. C. Liu, P. F. Nealey, K. Char, *Macromolecules* **2010**, *43*, 461–466.
- R. Ruiz, R. L. Sandstrom, C. T. Black, *Adv. Mater.* **2007**, *19*, 587–590.
- S. Ji, C. C. Liu, W. Liao, A. L. Fenske, G. S. W. Craig, P. F. Nealey, *Macromolecules* **2011**, *44*, 4291–4300.
- C. Harrison, D. H. Adamson, Z. D. Cheng, J. M. Sebastian, S. Sethuraman, D. A. Huse, R. A. Register, P. M. Chaikin, *Science* **2000**, *290*, 1558–1560.
- C. Harrison, Z. D. Cheng, S. Sethuraman, D. A. Huse, P. M. Chaikin, D. A. Vega, J. M. Sebastian, R. A. Register, D. H. Adamson, *Phys. Rev. E* **2002**, *66*, 011706.
- R. A. Segalman, A. Hexemer, R. C. Hayward, E. J. Kramer, *Macromolecules* **2003**, *36*, 3272–3288.
- M. Hammond, E. Cochran, G. Fredrickson, E. Kramer, *Macromolecules* **2005**, *38*, 6575–6585.
- D. E. Angelescu, J. H. Waller, D. H. Adamson, P. Deshpande, S. Y. Chou, R. A. Register, P. M. Chaikin, *Adv. Mater.* **2004**, *16*, 1736–1739.
- S. Pujari, M. A. Keaton, P. M. Chaikin, R. A. Register, *Soft Matter* **2012**, *8*, 5358–5363.
- T. Hashimoto, J. Bodycomb, Y. Funaki, K. Kimishima, *Macromolecules* **1999**, *32*, 952–954.
- J. Bodycomb, Y. Funaki, K. Kimishima, T. Hashimoto, *Macromolecules* **1999**, *32*, 2075–2077.
- D. E. Angelescu, J. H. Waller, D. H. Adamson, R. A. Register, P. M. Chaikin, *Adv. Mater.* **2007**, *19*, 2687–2690.
- B. C. Berry, A. W. Bosse, J. F. Douglas, R. L. Jones, A. Karim, *Nano Lett.* **2007**, *7*, 2789–2794.
- C. Tang, W. Wu, D. M. Smilgies, K. Matyjaszewski, T. Kowalewski, *J. Am. Chem. Soc.* **2011**, *133*, 11802–11809.
- G. Singh, K. G. Yager, D. M. Smilgies, M. M. Kulkarni, D. G. Bucknall, A. Karim, *Macromolecules* **2012**, *45*, 7107–7117.
- R. A. Segalman, H. Yokoyama, E. J. Kramer, *Adv. Mater.* **2001**, *13*, 1152–1155.
- J. Y. Cheng, C. A. Ross, E. L. Thomas, H. I. Smith, G. J. Vancso, *Appl. Phys. Lett.* **2002**, *81*, 3657–3659.
- I. Bitá, J. K. W. Yang, Y. S. Jung, C. A. Ross, E. L. Thomas, K. K. Berggren, *Science* **2008**, *321*, 939–943.
- J. Y. Cheng, D. P. Sanders, H. D. Truong, S. Harrer, A. Friz, S. Holmes, M. Colburn, W. D. Hinsberg, *ACS Nano* **2010**, *4*, 4815–4823.
- L. Rockford, Y. Liu, P. Mansky, T. Russell, M. Yoon, S. Mochrie, *Phys. Rev. Lett.* **1999**, *82*, 2602–2605.
- X. Yang, R. Peters, P. Nealey, H. Solak, F. Cerrina, *Macromolecules* **2000**, *33*, 9575–9582.
- S. O. Kim, H. H. Solak, M. P. Stoykovich, N. J. Ferrier, J. J. de Pablo, P. F. Nealey, *Nature* **2003**, *424*, 411–414.
- M. P. Stoykovich, M. Muller, S. O. Kim, H. H. Solak, E. W. Edwards, de J. J. Pablo, P. F. Nealey, *Science* **2005**, *308*, 1442–1446.

- 40** M. P. Stoykovich, H. Kang, K. C. Daoulas, G. Liu, C. C. Liu, J. J. de Pablo, M. Mueller, P. F. Nealey, *ACS Nano* **2007**, *1*, 168–175.
- 41** G. E. Stein, J. A. Liddle, A. L. Aquila, E. M. Gullikson, *Macromolecules* **2010**, *43*, 433–441.
- 42** G. Perera, C. Wang, M. Doxastakis, R. Kline, W. Wu, A. Bosse, G. Stein, *ACS Macro Lett.* **2012**, *1*, 1244–1248.
- 43** J. K. Bosworth, E. A. Dobisz, O. Hellwig, R. Ruiz, *Macromolecules* **2011**, *44*, 9196–9204.
- 44** International Technology Roadmap for Semiconductors; 2011; (Chapter titled Lithography). Available at <http://www.itrs.net/Links/2011ITRS/Home2011.htm>.
- 45** P. Mueller-Buschbaum, E. Maurer, E. Bauer, R. Cubitt, *Langmuir* **2006**, *22*, 9295–9303.
- 46** G. Stein, E. Kramer, X. Li, J. Wang, *Macromolecules* **2007**, *40*, 2453–2460.
- 47** P. Mueller-Buschbaum, L. Schulz, E. Metwalli, J. F. Moulin, R. Cubitt, *Langmuir* **2008**, *24*, 7639–7644.
- 48** V. Mishra, S. M. Hur, E. Cochran, G. Stein, G. Fredrickson, E. Kramer, *Macromolecules* **2010**, *43*, 1942–1949.
- 49** T. Xu, C. J. Hawker, T. P. Russell, *Macromolecules* **2005**, *38*, 2802–2805.
- 50** K. G. Yager, B. C. Berry, K. Page, D. Patton, A. Karim, E. J. Amis, *Soft Matter* **2009**, *5*, 622–628.
- 51** D. Korolkov, P. Busch, L. Willner, E. Kentzinger, U. Ruecker, A. Paul, H. Frielinghaus, T. Brueckel, *J. Appl. Crystallogr.* **2012**, *45*, 245–254.
- 52** G. Renaud, R. Lazzari, F. Leroy, *Surf. Sci. Rep.* **2009**, *64*, 255–380.
- 53** Z. Jiang, D. Lee, S. Narayanan, J. Wang, S. Sinha, *Phys. Rev. B* **2011**, *84*.
- 54** X. Lu, K. G. Yager, D. Johnston, C. T. Black, B. M. Ocko, *J. Appl. Crystallogr.* **2012**, in press.
- 55** A. M. Welander, H. Kang, K. O. Stuen, H. H. Solak, M. Mueller, de J. J. Pablo, P. F. Nealey, *Macromolecules* **2008**, *41*, 2759–2761.
- 56** Z. Jiang, X. Li, J. Strzalka, M. Sprung, T. Sun, A. R. Sandy, S. Narayanan, D. R. Lee, J. Wang, *J. Synchrotron Radiat.* **2012**, *19*, 627–636.
- 57** G. Stein, E. Kramer, X. Li, J. Wang, *Phys. Rev. Lett.* **2007**, *98*, 086101.
- 58** Z. Jiang, X. M. Lin, M. Sprung, S. Narayanan, J. Wang, *Nano Lett.* **2010**, *10*, 799–803.
- 59** B. Lee, I. Park, J. Yoon, S. Park, J. Kim, K. Kim, T. Chang, M. Ree, *Macromolecules* **2005**, *38*, 4311–4323.
- 60** P. Busch, M. Rauscher, J. F. Moulin, Mueller-Buschbaum, P. *J. Appl. Crystallogr.* **2011**, *44*, 370–379.
- 61** J. Bang, B. Kim, G. Stein, T. Russell, X. Li, J. Wang, E. Kramer, C. Hawker, *Macromolecules* **2007**, *40*, 7019–7025.
- 62** L. Parratt, *Phys. Rev.* **1954**, *95*, 359–369.
- 63** We convolve the intensity with a Gaussian line shape to account for the finite in-plane correlation length, or small grain size.
- 64** Y. Yoneda, *Phys. Rev.* **1963**, *131*, 2010–2013.
- 65** When moving the vacuum sample chamber along the x-axis, strain on the vacuum bellows could cause misalignment of the guard slits and parasitic scattering. This complication is unique to the beamline in question. However, all GI-SAXS experiments rely on a precise z-stage for sample alignment, while tuning sample alignment along the x-axis is less common.
- 66** Increasing the incident angle will further reduce the reflection coefficient, but the reduced path length will produce a weaker transmitted signal.
- 67** C. Harrison, P. M. Chaikin, D. A. Huse, R. A. Register, D. H. Adamson, A. Daniel, E. Huang, P. Mansky, T. P. Russell, C. J. Hawker, D. A. Egolf, I. V. Melnikov, E. Bodenschatz, *Macromolecules* **2000**, *33*, 857–865.
- 68** M. Konrad, A. Knoll, G. Krausch, R. Magerle, *Macromolecules* **2000**, *33*, 5518–5523.
- 69** E. Sivaniah, Y. Hayashi, S. Matsubara, S. Kiyono, T. Hashimoto, K. Kukunaga, E. J. Kramer, T. Mates, *Macromolecules* **2005**, *38*, 1837–1849.